

Permeation and thermal desorption model of hydrogen in steel: a sensitivity analysis

Paolo Emilio Di Nunzio
RINA Consulting - Centro Sviluppo Materiali S.p.A.,
Via di Castel Romano 100, 00128 Rome, ITALY
paolo.dinunzio@rina.org - ORCID: 0000-0001-8260-6644

Abstract

This work presents a fully physical model of the hydrogen diffusion and trapping kinetics in metals, integrating permeation and thermal desorption within a unified framework. Based on the McNabb and Foster approach, it requires only binding energy and number density of trap sites. It correctly reproduces the physics of the system and the results of the analytical solutions of the permeation kinetics. It is also capable of reproducing thermal desorption spectra with considerable accuracy.

The sensitivity analysis has elucidated the relationships among the processing conditions and the parameters commonly used to characterize permeation and thermal desorption experiments. An equation empirically derived from the simulation results, expressing the dependence of time lag in desorption on specimen thickness, number density of occupied trap sites, and cathodic concentration, is proposed.

In summary, the model represents a valuable tool in supporting the interpretation and rationalization of experiments also from a quantitative viewpoint.

Keywords

Hydrogen, Trapping, Permeation, Thermal Desorption, Kinetics

Highlights

- Fully physical model of the hydrogen diffusion and trapping kinetics in metals
- Same theoretical framework adopted for permeation and thermal desorption
- The sensitivity analysis revealed correlations between processing conditions and model results
- Empirical equation proposed to relate time lag to occupied trap sites and cathodic concentration

Introduction

The emerging view of hydrogen as a widespread energy source demands increasing efforts to address the long-standing issues related to the brittleness it induces in steels used for its transportation and storage [1]. Therefore, the development of modeling tools to interpret and rationalize experimental evidence is particularly important.

The scope of this work is the development of a fully physical model of the diffusion and trapping kinetics of hydrogen in metals to describe both permeation and thermal desorption experiments within a unified theoretical framework. The model, based on the approach outlined by McNabb and Foster [2], ideally requires no calibration parameters other than the binding energy and number density of the different trap sites present within the system.

Obviously, it must reproduce the features of the consolidated theoretical analyses and experiments. To this end, a comprehensive sensitivity analysis is carried out to assess its capabilities and its internal consistency. It is hoped that the statistical foundation on which the model has been built could offer further insights into the basic mechanisms governing the process.

The model, as here presented, is specific for body-centered cubic (bcc) iron but can be readily adapted to any structure by simply updating the crystallography-related data and diffusion coefficients.

The approach, based on the original formulation by McNabb and Foster [2], considers the adsorption and desorption kinetics on the traps as separate processes. Each elementary process is characterized by its own activation energy, and both are in equilibrium with the diffusible hydrogen residing in the lattice sites of the matrix. The flux of diffusible hydrogen through the specimen is governed by the concentration gradients arising from the boundary conditions. Regarding the equilibration of solute hydrogen with traps, the Oriani hypothesis [3] is assumed to hold. It posits that the characteristic time for establishing the equilibrium between lattice and trap sites is much shorter than that for lattice diffusion of hydrogen. It is important to note that the Oriani approach, as defined, is appropriate for interpreting permeation experiments under the assumption that all traps are reversible. Consequently, it is not directly applicable for describing thermal desorption phenomena when irreversible traps are present. In fact, at any time, the equilibrium between traps and lattice is complete and instantaneous, even for high energy traps because the equilibrium occupancy fraction of trap sites y_T is linearly dependent on the occupancy fraction of lattice sites y_L through the trap energy E_T :

$$y_T = \frac{y_L \cdot \exp\left\{+\frac{E_T}{RT}\right\}}{1 + y_L \cdot \exp\left\{+\frac{E_T}{RT}\right\}} \quad (1)$$

This implies that when the lattice concentration of hydrogen falls to zero, a complete desorption from all traps occurs even at room temperature. However, in real systems, some hydrogen remains bound to irreversible traps even after prolonged spontaneous desorption at low temperature. In such cases, the desorption kinetics are not suppressed; instead, they are proportionally slowed down as the trap energy increases. Only by raising the temperature or by applying a heating ramp at a constant rate, it is possible to obtain a thermal desorption spectrum (TDS) where the outflowing hydrogen peaks appear at temperatures correlated with the corresponding trap energies.

Numerous approaches can be found in the literature where similar models are presented, but these are often applied exclusively to either permeation or thermal desorption. Furthermore, their formulation frequently employs calibration coefficients for the reaction rates or relies on equations that are not explained in detail [4], [5], [6], [7], [8], [9], [10], [11], [12], [13], [14], [15], [16].

Moreover, it has been observed that in some literature models describing thermal desorption spectra, the desorption peaks tend to be concentrated at low temperatures, even for high-energy traps. A potential explanation for this effect is an overestimation of the detrapping kinetics, presumably caused by an inadequate balance of the reaction rates. The present

formulation attempts to address this issue by employing elementary statistical arguments to modulate the reaction rates of trap adsorption and desorption.

Formulation of the model

Diffusible hydrogen is assumed to occupy the 12 tetrahedral interstitial sites of the bcc iron lattice. Their number per unit volume, N_L [m^{-3}], is deduced from its crystal structure as shown later in Equation (12a). The hydrogen concentration, c_L [m^{-3}], is calculated from the fraction of occupancy y_L as:

$$c_L = y_L \cdot N_L \quad (2)$$

Similarly, the concentration in the traps of type j is:

$$c_{Tj} = y_{Tj} \cdot N_{Tj} \quad (3)$$

where correspondingly, y_{Tj} is the occupancy fraction and N_{Tj} their spatial density.

The total concentration of hydrogen in the steel is the sum of the contributions from lattice and all trap types:

$$c_{tot} = y_L \cdot N_L + \sum_j y_{Tj} \cdot N_{Tj} \quad (4)$$

The specimen is a thin sheet of thickness L with plane-parallel surfaces, as that used in permeation experiments according to the Devanathan-Stachurski method [17], [18] adopted in the ASTM G148-97 and ISO 17081:2004 standards. The hydrogen flux is assumed to take place only parallel to its thickness, along the spatial coordinate z .

It is also assumed with good approximation that $N_L \gg \sum_j N_{Tj}$, namely that the density of lattice sites is much greater than the sum of all trap sites. In fact, a realistic estimation permits to evaluate the order of magnitude of the ratio as $\sum_j N_{Tj} / N_L \sim 10^{-4}$. Consequently, the transition probability between traps of different kinds can be considered negligible.

The overall equation is a mass balance between the adsorption and desorption kinetics and the lattice diffusion described by the second Fick's law. It is more conveniently expressed in terms of concentration rather than occupancy fraction as:

$$\frac{dc_L}{dt} = D_H \frac{\partial^2 c_L}{\partial z^2} - \sum_j \frac{dc_j^{in}}{dt} + \sum_j \frac{dc_j^{out}}{dt} \quad (5)$$

where D_H is the diffusion coefficient in absence of traps.

For traps of j -th type, the kinetic equations for the elementary steps of adsorption and desorption are, respectively:

$$\frac{dc_j^{in}}{dt} = \left[\frac{kT}{h} \cdot \frac{N_L}{N_L + \sum_k N_{Tk}} \right] \cdot N_{Tj} \cdot \left[y_L \cdot (1 - y_{Tj}) \cdot \exp \left\{ -\frac{Q_D}{RT} \right\} \right] \quad (6a)$$

$$\frac{dc_j^{out}}{dt} = \left[\frac{kT}{h} \cdot \frac{N_{Tj}}{N_L + \sum_k N_{Tk}} \right] \cdot N_{Tj} \cdot \left[y_{Tj} \cdot (1 - y_L) \cdot \exp \left\{ -\frac{Q_D + E_{Tj}}{RT} \right\} \right] \quad (6b)$$

They consist of different factors which have been grouped in brackets for clarity. The first one contains the pre-factor kT/h , an estimate of the lattice vibration frequency according to Eyring [19], and a term expressing the fraction of sites in the system from which the transition starts. In the adsorption equation the starting sites belong to the lattice ($L \rightarrow T_j$), in the desorption equation they belong to the traps of j -th type ($T_j \rightarrow L$). The Eyring factor is preferred over the Debye frequency, a constant of the same order of magnitude, often used in similar models in the literature, because it incorporates fundamental physical constants and an additional temperature dependence. Consequently, the overall number of jumps in the unit time is partitioned among lattice and trap sites according to their respective fraction in the system. Practically, in the case of adsorption, being $N_L \gg \sum_j N_{Tj}$, one has $N_L / (N_L + \sum_j N_{Tj}) \cong 1$. Conversely, in the desorption equation the fraction is consequently smaller by at least one or two orders of magnitude. This factor plays a central role in reducing the rate of desorption from the traps, thereby allowing a slow spontaneous desorption at room temperature and the persistence of hydrogen in the steel for a long time, especially for high energy traps.

The last term represents the transition probability of independent events, modulated by an Arrhenius-type term. The pre-exponential factor is the product probability of finding an occupied place at the starting site and a free place at the destination. The exponential term provides information on the activation energy of the process and is asymmetrical. For the adsorption step the activation barrier Q_D is the same as that for bulk diffusion (see equation (13) later), while for the reverse process, the quantity $Q_D + E_{Tj}$ represents the combination between the previous one and the proper trap energy, as sketched in Figure 1.

Finally, the intermediate factor, N_{Tj} , expresses a proximity condition. Transitions from lattice to traps and *vice versa* can occur only between adjacent sites in the system. Since the spatial density of lattice sites is orders of magnitude greater than that of trap sites, the process is controlled by the density of trap sites in both equations.

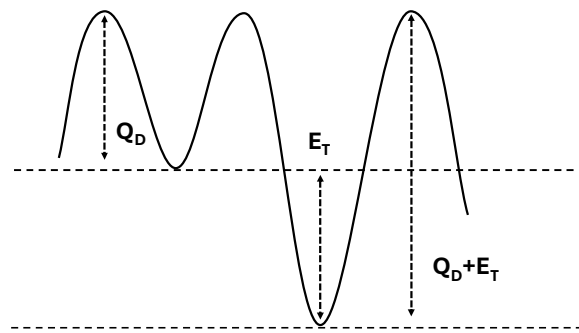


Figure 1 Schematic energy diagram for trapping and detrapping processes: Q_D is the activation energy for adsorption and bulk diffusion, $Q_D + E_T$ that for desorption.

Numerical solution of the diffusion equation

The specimen thickness is subdivided into $n+1$ nodes ($i=0, \dots, n$) evenly spaced by Δz . Nodes 0 and n are located on the external surfaces where constant boundary conditions are

imposed based on the process to be simulated. During permeation node 0 is the cathodic side where hydrogen enters the metal, and node n is the anodic side where hydrogen is extracted from. In this case the boundary conditions are $c(0) = c_0$ and $c(n) = 0$. At the end of charging, hydrogen is let to desorb from both the specimen surfaces and the boundary conditions become $c(0) = c(n) = 0$. The equation is integrated numerically using an explicit finite difference scheme.

For the inner nodes ($i=1, \dots, n-1$) the lattice concentration at the time $t + \Delta t$ is calculated from the balance:

$$c_{L,i}(t + \Delta t) = c_{L,i}(t) - \Delta c_i^{in} + \Delta c_i^{out} + \Delta c_{L,i} \quad (7)$$

where

$$\Delta c_i^{in} = \sum_j \Delta c_{j,i}^{in} = \Delta t \cdot \sum_j \frac{dc_{j,i}^{in}}{dt} \quad (8a)$$

$$\Delta c_i^{out} = \sum_j \Delta c_{j,i}^{out} = \Delta t \cdot \sum_j \frac{dc_{j,i}^{out}}{dt} \quad (8b)$$

are the contributions from all traps in the time step, and

$$\Delta c_{L,i} = \frac{\Delta t}{\Delta z^2} \cdot D_H \cdot [c_{L,i-1}(t) - 2c_{L,i}(t) + c_{L,i+1}(t)] \quad (9)$$

is the lattice diffusion contribution in the time step.

A variable time step Δt must be carefully chosen to provide a correct coupling between lattice diffusion and trapping kinetics and to guarantee a numerically stable solution. The first constraint is the classical von Neumann stability condition $\Delta t \leq \Delta z^2 / (2 D_H)$ valid for bulk diffusion. The most demanding aspect is related to the trapping-detrapping kinetics which, according to the Oriani assumption, is much faster than diffusion. Therefore, before calculating the flux of diffusible hydrogen in the matrix, the mass balance on traps must be evaluated.

For a given node i and a given time, the integration time step Δt_i is the maximum value that satisfies the mass balance. The time step to be applied to the entire set of nodes is the absolute minimum among them: $\Delta t = \min(\Delta t_i)$. This ensures that the whole system evolves consistently and synchronously.

The fulfilment of mass balance constraints must be continuously monitored. The related conditions are readily obtained from elementary arguments, as the number of hydrogen atoms transitioning from lattice to the j -th trap ($L \rightarrow T_j$) or from trap to lattice ($T_j \rightarrow L$) must always be less than or equal to the number of free sites available at the destination and, at the same time, less than or equal to the occupied sites at the starting location. With reference to the trap sites, the following conditions must be fulfilled for each node i :

$$\Delta c_j^{in} \leq c_L ; \Delta c_j^{in} \leq N_{Tj}(1 - y_{Tj}) \quad (10a)$$

$$\Delta c_j^{out} \leq c_{Tj} ; \Delta c_j^{out} \leq N_L(1 - y_L) \quad (10b)$$

Finally, the hydrogen flux from n -th node, expressed in g/m²/s, is calculated as:

$$J_{out}(t) = m_H \cdot \frac{D_H}{\Delta z} \cdot [c_{Li-1}(t) - c_{Li}(t)] \quad (11)$$

where $m_H = 1.67328 \cdot 10^{-24}$ g is the mass of one atom and $c_{Li}(t) = 0$ as boundary condition. A similar relationship holds for the 0-th node during free and thermal desorption.

Density of trap sites

Evaluations of trap density can be found in the literature, such as for example in Song et al. [7]. Nevertheless, the approximate estimation of the density [m⁻³] of various types of sites here reported is based on the crystal structure of bcc iron (lattice parameter $a=0.286$ nm) and on the geometrical properties of the microstructural features involved:

$$\text{Lattice sites (tetrahedral):} \quad N_L = 12/a^3 \quad (12a)$$

$$\text{Grain boundaries:} \quad N_{GB} = \frac{3.35}{\langle D \rangle a^2} \quad (12b)$$

$$\text{Dislocations:} \quad N_{Disl} = \frac{\rho_{Disl}}{a} \quad (12c)$$

$$\text{Precipitates:} \quad N_{Prec} = \frac{N_{vp}}{a^2} \cdot \pi d_p^2 = \frac{6 f_{vp}}{d_p a^2} \quad (12d)$$

where $\langle D \rangle$ is the mean size of grains with shape of tetrakaidekahedra according to Capdevila et al. [20], ρ_{Disl} is the dislocation density, d_p and f_{vp} are the mean size of spherical particles and their volume fraction, respectively. The latter quantities are related to the number density of precipitates through the following relationship: $N_{vp} = 6 f_{vp} / \pi d_p^3$.

The density of trap sites from the above expressions, except for lattice sites, should be considered a theoretical upper limit. Possible interactions among hydrogen atoms on adjacent sites, which might reduce the actual maximum occupancy, have been neglected. Nonetheless, the orders of magnitudes of the estimates can be considered correct.

Trap energy

A substantial body of literature exists on the classification of traps and their associated binding energies. Following the first works of Pressuyre and Bernstein [21], [22] and Hirth [23], numerous analyses and new determinations have been published, including those by Choo and Lee [24], Lee and Lee [25], Hagi and Hayashi [26], Parvathavarthini et al. [27], Asahi et al. [28], Wei et al. [29], Frappart et al. [30], Gaude-Fugarolas [31], and Sanchez et al [32].

Notably, the recent comprehensive review by Chen et al. [33] provides a synthetic overview summarized in Table 1.

Table 1 Binding energy ranges of the main trap types in ferrite from the work by Chen et al. [33].

Trap type	Binding energy (kJ/mol)
High angle grain boundaries	10-60
Dislocation field	10-30
Ferrite/cementite interface	10-20
Ferrite/austenite interface	45
Coherent TiC	20-25
Incoherent TiC	85-95
Semicoherent NbC	10-65
Incoherent NbC	55-60

Diffusion coefficient of hydrogen in ferrite

The diffusion coefficient of hydrogen in ferrite has been taken from Kiuchi et al. [34] as quoted by the excellent review by Turnbull [35]:

$$D_H(m^2/s) = 7.23 \cdot 10^{-8} \cdot \exp \left\{ -\frac{5.69 \text{ kJ/mol}}{RT} \right\} \quad (13)$$

Strictly speaking, the expression is valid for temperatures below approximately 80°C where hydrogen occupies only tetrahedral sites. At higher temperatures (e.g. during thermal desorption) octahedral sites also become populated and a different diffusion coefficient should be considered. In the simulations presented here, it has been assumed that the above coefficient can be extrapolated above room temperature.

Calculations

The sensitivity analysis has been conducted by performing simulations with specimen thicknesses of 0.25, 0.5 and 1 mm and varying the cathodic concentration of hydrogen from 0.01 to 0.5 ppm, a range consistent with some calculations reported in the literature [36], [37], [38], [39].

Although the model can in principle handle any number of different trap types, each one characterized by a binding energy and a density of sites, the simplified system considered for this sensitivity analysis includes only two types of traps: reversible traps with a binding energy of 20 kJ/mol, ideally associated with grain boundaries, and irreversible traps with energy in the range 40 to 70 kJ/mol, ideally associated with precipitates.

The typical calculation consists of a permeation stage up to the stationary condition, a free desorption stage long enough to allow the desorption of almost all the reversible traps, both carried out at a temperature of 25°C, and a thermal desorption stage with heating rates of 100, 250 or 500°C/h.

In the first group of simulations, the permeation and free desorption kinetics are considered. In the second group the focus is on the application of the Kissinger analysis for recovering the trap energy from thermal desorption kinetics at different heating rates.

A number of nodes, ranging from 5 to 10 depending on the specimen thickness, has been used for integrating the diffusion equations. During permeation, the cathodic concentration c_0 is imposed as boundary condition while on the opposite side the concentration is set to zero. During free desorption, hydrogen is let to escape from both the specimen surfaces. The exit flux, expressed in g/m²/s, is averaged over time intervals of 30 seconds to reduce the numerical noise deriving from the kinetics of trap equilibration.

Simulation of permeation experiments

Permeation tests have been simulated to determine the dependence of time lag t_L , maximum permeation flux J_∞ , maximum *average* hydrogen concentration c_{max} during the stationary state on the cathodic concentration, density of reversible and irreversible traps and specimen thickness L . The model also allows for determining the residual average concentration of hydrogen at the end of free desorption (c_{min}) and the average occupancy fraction of traps over time. The temperature of the thermal desorption peak of irreversible traps is also considered. It should be noted that the minimum residual concentration calculated by the model, which measures the number of irreversible traps per unit volume, can fluctuate slightly depending on the duration of the free desorption stage relative to the specimen thickness due to incomplete desorption of the reversibly trapped hydrogen.

The time lag is determined numerically from the plot of the integrated flux versus time by finding the stationary regime, i.e. the onset of the linearity region corresponding to the maximum constant permeation flux J_∞ , and calculating the position of the intercept on the time axis of the fitted straight line.

The first set of simulations has been performed with $L=0.25, 0.5$ and 1 mm, a density of reversible traps $N_{rev}=4.1 \cdot 10^{24} \text{ m}^{-3}$ ($E_{rev}=20 \text{ kJ/mol}$), of irreversible traps $N_{irrev}=1.75 \cdot 10^{23} \text{ m}^{-3}$ ($E_{irrev}=60 \text{ kJ/mol}$) and a heating rate in desorption of 250°C/h . The cathodic concentration has been varied from 0.01 to 0.5 ppm. The results are reported in Table 2.

Table 2 Effect of the cathodic concentration c_0 on the main permeation and thermal desorption parameters for a fixed density of reversible ($4.1 \cdot 10^{24} \text{ m}^{-3}$, $E_{rev}=20 \text{ kJ/mol}$), and irreversible traps ($N_{irrev}=1.75 \cdot 10^{23} \text{ m}^{-3}$, $E_{irrev}=60 \text{ kJ/mol}$).

L (mm)	c_0 (ppm)	t_L (s)	J_∞ (g/m ² /s)	c_{max} (ppm)	c_{min} (ppm)	$T(20 \text{ kJ/mol})$ (°C)	$T(60 \text{ kJ/mol})$ (°C)
0.25	0.01	3969	$4.13 \cdot 10^{-8}$	12.1	1.86	-	463.4
0.25	0.05	2022	$2.06 \cdot 10^{-7}$	26.9	1.86	-	463.4
0.25	0.10	1294	$4.13 \cdot 10^{-7}$	33.1	1.86	-	463.4
0.25	0.25	639	$1.03 \cdot 10^{-6}$	39.1	1.86	-	463.4
0.25	0.50	350	$2.06 \cdot 10^{-6}$	42.0	1.86	-	463.4
0.5	0.01	14635	$2.03 \cdot 10^{-8}$	12.1	1.87	-	544.8
0.5	0.05	8079	$1.03 \cdot 10^{-7}$	26.9	1.88	139.8	550.0
0.5	0.10	4959	$2.06 \cdot 10^{-7}$	33.1	1.97	131.5	544.8
0.5	0.25	2555	$5.16 \cdot 10^{-7}$	39.1	1.97	131.5	544.8
0.5	0.50	1401	$1.03 \cdot 10^{-6}$	42.0	1.97	131.4	544.8
1.0	0.01	63418	$1.02 \cdot 10^{-8}$	12.1	2.51	153.3	652.4
1.0	0.05	31435	$5.16 \cdot 10^{-8}$	26.9	3.00	195.9	651.8
1.0	0.10	18357	$1.03 \cdot 10^{-7}$	33.1	3.10	195.7	651.8
1.0	0.25	10219	$2.58 \cdot 10^{-7}$	39.1	4.86	192.8	651.1
1.0	0.50	5605	$5.16 \cdot 10^{-7}$	42.0	4.88	192.7	651.1

The saturation flux on the anodic side during permeation increases linearly with the cathodic concentration, as shown in Figure 2. This result is obtained also when a system containing reversible traps only ($E_T=20 \text{ kJ/mol}$) is considered. The linearity is a direct consequence of the first Fick's law because in stationary conditions, a linear hydrogen concentration gradient across the specimen thickness is established between the limits c_0 and 0, so that one can write:

$$J_\infty = D_H \cdot \frac{c_0}{L} \quad (14)$$

where the concentration is expressed in g/m³. The above relationship can be used to estimate the cathodic concentration from the stationary flux (g/m²/s) obtained from the experiments as:

$$c_0(ppm) = \frac{10^3}{\rho_{Fe}} \cdot \frac{J_\infty L}{D_H} \quad (15)$$

In fact, when the saturation flux is reached, the trapping-detrapping kinetics are in a stationary regime for all types of traps. Thus, the trap occupancy fraction remains constant, even if it is less than unity. Consequently, only the diffusible hydrogen in the lattice contributes to the permeation flux on the anodic side.

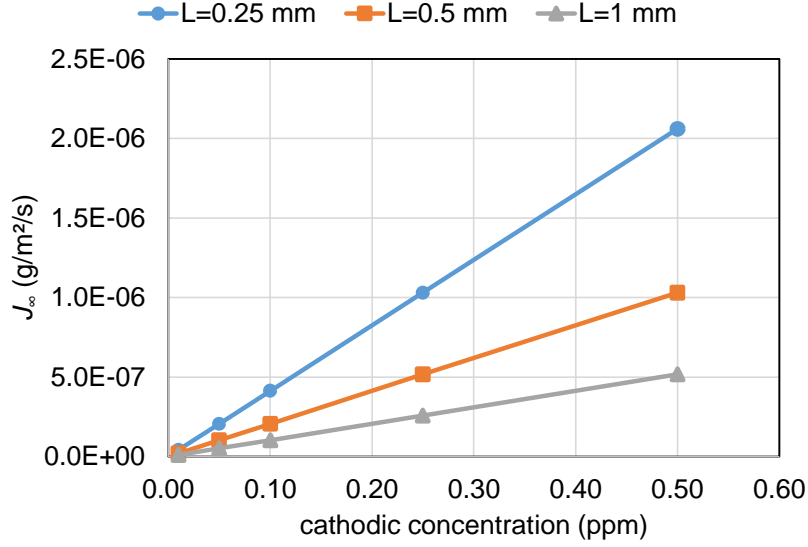


Figure 2 Stationary permeation flux as a function of the cathodic hydrogen concentration and of the specimen thickness.

In his work, Oriani [Ori70] reports a similar expression to estimate the subsurface concentration on the cathodic side,

$$c_0^* = \frac{J_{\infty} L}{D_{app}} \quad (16)$$

where the apparent diffusion coefficient of hydrogen ($D_{app} = L^2/6 t_L$) is used instead of the trap-free diffusion coefficient D_H . As noted by Oriani and emphasized by Turnbull [35], this relationship holds only if reversible traps dominate over irreversible ones and the occupancy of reversible trap sites is small enough for the second Fick to be applied across the entire thickness. In such a condition the concentration c_0^* , deduced using D_{app} , represents the sum of hydrogen atoms in lattice sites and reversible traps.

Although in principle this quantity is theoretically associated with reversible traps, it is interesting to compare the concentration c_0^* as defined by Oriani with the minimum residual hydrogen concentration calculated by the model at the end of the free desorption stage at room temperature (just before starting the thermal desorption stage), which is instead related to irreversibly trapped hydrogen. Both are reported in Table 3 with reference to the simulations in Table 2. The agreement is generally satisfactory, except for some overestimations in the thicker specimens, where the residual flux was greater than 10^{-10} g/m²/s. In such cases, as previously said, the free desorption time has not been long enough to allow complete escape of hydrogen from reversible traps.

This result suggests that equation (16) may address not only reversible traps but also the contribution of irreversible ones, which, although generally present at lower concentrations, are fully saturated and influence the time lag as well.

To attempt an analysis of this result, equation (16) is reformulated by substituting $L^2/6 t_L$ for the apparent diffusion coefficient and J_{∞} from equation (14) and rearranging to obtain an expression where the dependence on cathodic concentration and time lag is evidenced:

$$c_0^* = \frac{6 D_H}{L^2} \cdot c_0 t_L \quad (17)$$

Thus, equation (17) can be used to relate the time lag to the ratio c_0^*/c_0 , as it will be shown in equation (21) in the discussion.

Table 3 Comparison between the concentration of trapped hydrogen according to Oriani and the minimum concentration calculated by the model at the end of free desorption at room temperature.

c_0 (ppm)	c_0^* (ppm)			c_{min} (ppm)		
	L=0.25 mm	L=0.5 mm	L=1 mm	L=0.25 mm	L=0.5 mm	L=1 mm
0.01	0.5	0.5	0.5	1.9	1.9	2.5
0.05	1.3	1.4	1.4	1.9	1.9	3.0
0.10	1.7	1.7	1.6	1.9	2.0	3.1
0.25	2.0	2.2	2.2	1.9	2.0	4.9
0.50	2.2	2.4	2.4	1.9	2.0	4.9

The maximum average concentration of hydrogen in the specimen under stationary permeation conditions increases with the saturation flux and tends towards an asymptote that is independent of specimen thickness. This maximum concentration reflects the combination of a variable occupancy degree of reversible traps, which increases with c_0 , and the full, constant occupancy of irreversible traps ($y_{irr}=1$), as illustrated in Figure 3. Thinner specimens achieve the same level of average maximum concentration at different saturation fluxes due to the inverse proportionality of J_∞ to specimen thickness. In fact, due to the linear relationship between c_0 and J_∞/L in equation (14), when c_{max} is plotted versus the cathodic concentration, all the curves overlap.

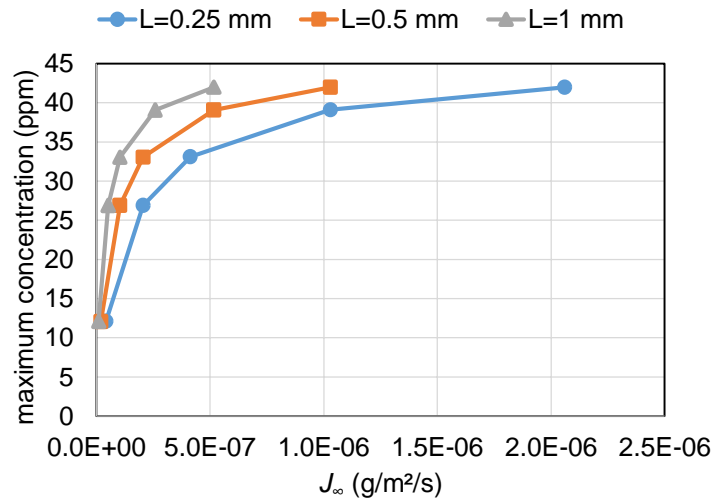


Figure 3 Maximum hydrogen concentration during the stationary permeation regime as a function of the saturation flux.

It is worth noting that the peak temperature of desorption for irreversible traps increases with the specimen thickness but shows negligible dependence on the cathodic concentration under the conditions imposed in Table 2. The peak associated with the reversible traps is not detected for the thinnest specimen because the free desorption stage before heating was sufficiently long to almost completely eliminate the reversibly trapped hydrogen.

A second set of simulations has been performed with a variable density of irreversible traps with $E_{irrev}=60$ kJ/mol, $L=0.25$, 0.5 and 1 mm, while keeping the density of reversible traps constant ($N_{rev}=4.1 \cdot 10^{24} \text{ m}^{-3}$, $E_{rev}=20$ kJ/mol), the cathodic concentration c_0 at 0.1 ppm and the desorption heating rate at 250°C/h. The results are reported in Table 4.

Table 4 Effect of the density of irreversible traps N_{irrev} on the main permeation and thermal desorption parameters for a fixed density of reversible traps and a cathodic concentration of 0.1 ppm.

L (mm)	N_{irrev} (m^{-3})	t_L (s)	J_∞ ($\text{g}/\text{m}^2/\text{s}$)	C_{max} (ppm)	C_{min} (ppm)	$T(20 \text{ kJ/mol})$ (°C)	$T(60 \text{ kJ/mol})$ (°C)
0.25	$3.50 \cdot 10^{20}$	1147	$4.13 \cdot 10^{-7}$	28.42	0.0034		759.4
0.25	$1.75 \cdot 10^{21}$	1148	$4.13 \cdot 10^{-7}$	28.44	0.0166		619.6
0.25	$3.50 \cdot 10^{21}$	1148	$4.13 \cdot 10^{-7}$	28.45	0.0331		572.8
0.25	$1.75 \cdot 10^{22}$	1154	$4.13 \cdot 10^{-7}$	28.58	0.165		500.7
0.25	$3.50 \cdot 10^{22}$	1161	$4.13 \cdot 10^{-7}$	28.75	0.33		487.3
0.25	$1.75 \cdot 10^{23}$	1218	$4.13 \cdot 10^{-7}$	30.07	1.65		478.6
0.25	$3.50 \cdot 10^{23}$	1289	$4.13 \cdot 10^{-7}$	31.72	3.30		476.8
0.25	$1.75 \cdot 10^{24}$	1856	$4.13 \cdot 10^{-7}$	44.92	16.50		477.9
0.5	$3.50 \cdot 10^{20}$	2907	$2.06 \cdot 10^{-7}$	18.01	0.060	130.8	747.1
0.5	$1.75 \cdot 10^{21}$	2910	$2.06 \cdot 10^{-7}$	18.02	0.075	130.8	624.4
0.5	$3.50 \cdot 10^{21}$	2913	$2.06 \cdot 10^{-7}$	18.04	0.093	130.8	587.5
0.5	$1.75 \cdot 10^{22}$	2938	$2.06 \cdot 10^{-7}$	18.19	0.242	130.9	549.0
0.5	$3.50 \cdot 10^{22}$	2970	$2.06 \cdot 10^{-7}$	18.37	0.427	130.9	548.1
0.5	$1.75 \cdot 10^{23}$	3226	$2.06 \cdot 10^{-7}$	19.86	1.91	132.6	549.0
0.5	$3.50 \cdot 10^{23}$	3545	$2.06 \cdot 10^{-7}$	21.72	3.77	143.0	549.8
0.5	$1.75 \cdot 10^{24}$	6085	$2.06 \cdot 10^{-7}$	36.57	18.60		550.0
1.0	$3.50 \cdot 10^{20}$	11628	$1.03 \cdot 10^{-7}$	18.01	1.50	192.8	788.8
1.0	$1.75 \cdot 10^{21}$	11638	$1.03 \cdot 10^{-7}$	18.02	1.51	192.7	669.6
1.0	$3.50 \cdot 10^{21}$	11651	$1.03 \cdot 10^{-7}$	18.04	1.53	192.8	628.9
1.0	$1.75 \cdot 10^{22}$	11753	$1.03 \cdot 10^{-7}$	18.19	1.68	191.6	618.8
1.0	$3.50 \cdot 10^{22}$	11881	$1.03 \cdot 10^{-7}$	18.37	1.86	191.6	631.1
1.0	$1.75 \cdot 10^{23}$	12901	$1.03 \cdot 10^{-7}$	19.86	3.35	192.8	652.4
1.0	$3.50 \cdot 10^{23}$	14175	$1.03 \cdot 10^{-7}$	21.72	5.20	191.8	628.2
1.0	$1.75 \cdot 10^{24}$	23674	$1.03 \cdot 10^{-7}$	36.57	20.10	198.7	615.7

Under these conditions, the peak temperature associated with the desorption of hydrogen from irreversible traps ($E_T=60$ kJ/mol) for a constant cathodic concentration depends on the density of trap sites, according to the data reported in Table 4. At low trap densities, the peak temperature is higher. As the trap density increases, the peak shifts to lower temperatures, eventually reaching an asymptotic value, as illustrated in Figure 4.

This indicates that the absolute position of a desorption is not solely associated with the trap energy; it also depends on trap density and heating rate, but not on cathodic concentration as demonstrated in the previous section.

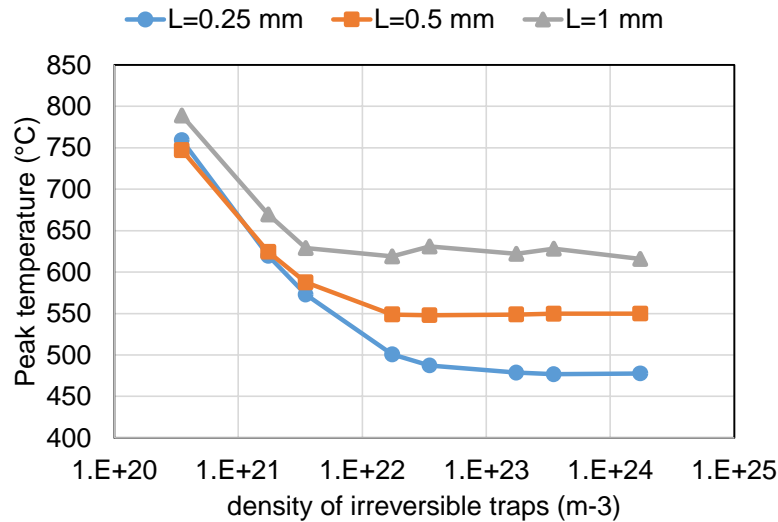


Figure 4 Calculated peak temperature of thermal desorption with heating rate of 250°C/h for irreversible traps of binding energy $E_T=60$ kJ/mol.

It is worth noting that in similar simulations conducted with binding energies of irreversible traps ranging from 40 to 70 kJ/mol, the time lag remains independent of the trap energy. This is because, within this range, all trap sites are saturated regardless of the specific binding energy.

Simulation of thermal desorption experiments

The effect of trap energy on the position of thermal desorption peaks is illustrated in Figure 5 for a specimen of thickness $L=0.25$ mm containing $4.10 \cdot 10^{24} \text{ m}^{-3}$ reversible trap sites with binding energy of 20 kJ/mol and $1.75 \cdot 10^{23} \text{ m}^{-3}$ irreversible trap sites. The binding energy of irreversible traps has been varied from 40 to 70 kJ/mol with a step of 10 kJ/mol. The simulations consisted of a permeation stage to saturate the traps with hydrogen, a free desorption stage to remove most of the irreversibly trapped hydrogen, and a thermal desorption stage with heating rate of 250°C/h.

The TDS exhibits two peaks: a small peak at about 130°C due to reversible traps with a binding energy of 20 kJ/mol, and a higher temperature peak associated with irreversible traps, which shifts to higher temperatures as the trap energy increases.

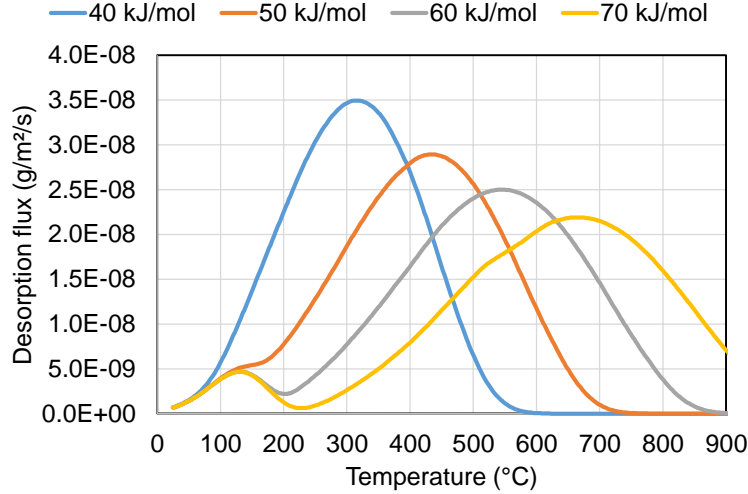


Figure 5 Effect of trap energy on the thermal desorption peak for $L=0.25$ mm and a heating rate of 250°C/h .

The total amount of hydrogen extracted from the specimen during thermal desorption is calculated by integrating the flux from both the desorbing surfaces, J_{tot} [g/m²/s], over the temperature ramp:

$$H_T(ppm) = \frac{1}{L} \cdot \frac{1000}{\rho_{Fe}} \cdot \frac{P_{Fe}}{P_H} \cdot \int J_{tot}(t) \cdot dt \quad (18)$$

where ρ_{Fe} is the steel density in kg/m³, L the specimen thickness (m), P_{Fe} and P_H the atomic mass of iron and hydrogen [g/mol] and the factor 1000 accounts for the conversion from grams to ppm mass.

The curves shown in Figure 6 illustrate the thermal desorption at 250°C/h of three specimens of thickness 0.25, 0.5 and 1.0 mm containing $4.10 \cdot 10^{24} \text{ m}^{-3}$ reversible trap sites with binding energy of 20 kJ/mol and $1.75 \cdot 10^{23} \text{ m}^{-3}$ irreversible trap sites with binding energy of 60 kJ/mol. A preliminary charging by permeation has been conducted by imposing a cathodic concentration of 0.1 ppm followed by a free desorption stage to remove as much of the reversibly trapped hydrogen as possible.

It can be observed that the desorption peaks of irreversible traps shift towards higher temperatures and broaden as the specimen thickness increases. For the thinnest sample, the desorption stage at room temperature has effectively removed the reversibly trapped hydrogen, as the first peak around 100°C is not observed.

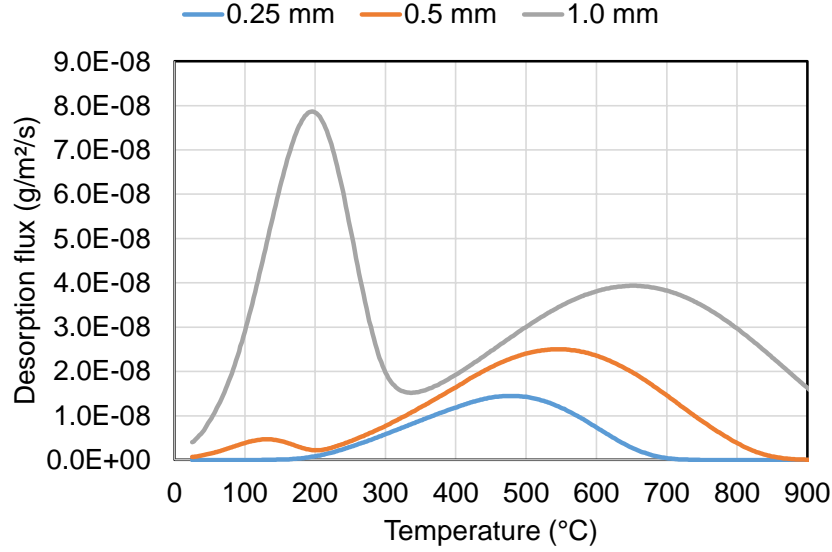


Figure 6 Effect of the specimen thickness on the thermal desorption peaks of reversible traps ($E_T=20$ kJ/mol) and irreversible traps ($E_T=60$ kJ/mol) for a heating rate of 250°C/h .

The numerical data for the position and full width at half maximum (FWHM) of the desorption peaks in Figure 6, along with the calculated peak areas and corresponding hydrogen content, are reported in Table 5. In the last two columns, the total amount of thermally desorbed hydrogen estimated by integration is compared with the minimum hydrogen content taken from the simulations at the end of the free desorption stage. The good agreement confirms the internal coherency of the model.

Table 5 Peak temperature, full width at half maximum, area and hydrogen content of reversible and irreversible traps as a function of the specimen thickness. The total amount of hydrogen is compared to the minimum amount at the end of free desorption.

L (mm)	T_{60} (°C)	FWHM ₆₀ (°C)	A_{60} (g/m ²)	C_{60} (ppm)	T_{20} (°C)	FWHM ₂₀ (°C)	A_{20} (g/m ²)	C_{20} (ppm)	A_{tot} (g/m ²)	C_{tot} (ppm)	C_{min} (ppm)
0.25	463	229	$5.96 \cdot 10^{-5}$	1.69			0	0.00	$5.96 \cdot 10^{-5}$	1.69	1.65
0.50	536	293	$1.35 \cdot 10^{-4}$	1.92	120	87	$6.54 \cdot 10^{-6}$	0.09	$1.41 \cdot 10^{-4}$	2.01	1.97
1.00	646	362	$2.33 \cdot 10^{-4}$	1.66	190	118	$1.56 \cdot 10^{-4}$	1.11	$3.89 \cdot 10^{-4}$	2.77	3.09

Kissinger analysis

In the previous section it has been shown that the position of the thermal desorption peaks is influenced not only by the trap energy but also by trap density and permeation conditions (L , c_0). Therefore, to reliably estimate the trap energy, the method developed by Kissinger [40] should be employed. It necessitates to carry out at least two thermal desorption experiments with different heating rates, starting from identical initial sample conditions. The trap energy corresponding to a specific desorption peak is calculated as:

$$d \left(\ln \frac{\dot{T}}{T_p^2} \right) / d \left(\frac{1}{T_p} \right) = - \frac{E_{des}}{R} \quad (19)$$

where \dot{T} is the heating rate, T_p the absolute temperature of the desorption peak, E_{des} the corresponding trap desorption energy and R the gas constant. The units used to measure the heating rate do not affect the result, as the slope of the straight line $\ln(\dot{T}/T_p^2)$ versus $1/T_p$ is evaluated.

As previously observed e.g. by Wang et al [12], it is important to note that the Kissinger method retrieves the energy associated with the desorption reaction, specifically:

$$E_{des} = E_T + Q_D \quad (20)$$

This will become evident from the analysis of the simulation data presented below.

A set of calculations has been performed to check the model response to the Kissinger analysis. Also in this case, a simple system consisting of two kinds of traps has been simulated. Reversible traps have been associated an energy of 20 kJ/mol, whereas for irreversible traps the energy has been varied between 40 kJ/mol to 80 kJ/mol.

A specimen thickness of 0.25 mm and a cathodic concentration from 0.01 to 0.5 ppm have been also considered. The density of reversible traps has been let to range from $2 \cdot 10^{24}$ to $4 \cdot 10^{24} \text{ m}^{-3}$, that of irreversible traps from 0 to $1.75 \cdot 10^{24} \text{ m}^{-3}$.

Three heating rates of thermal desorption (100, 250 and 500°C/h) have been applied to check for the expected linearity of the Kissinger equation which was found to be rigorously fulfilled in all cases. The results, plotted in Figure 7, show an excellent linear correlation with a slope of 1.03, indicating a moderate systematic overestimation of the nominal energy. When also the specimen thicknesses of 0.5 and 1 mm are considered, linearity is preserved but the data are slightly more dispersed.

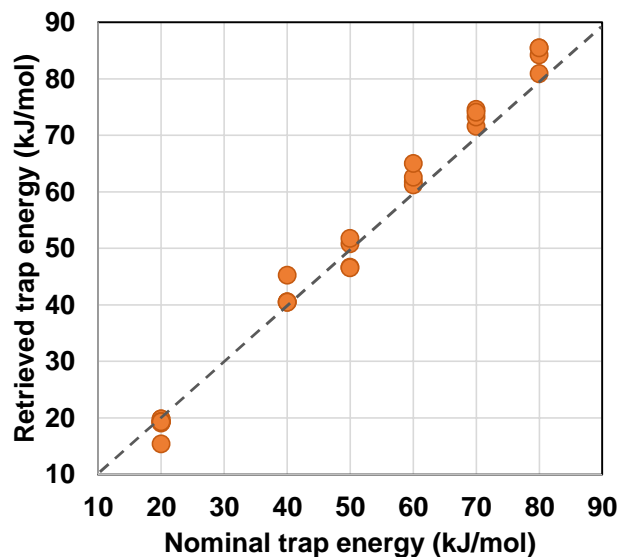


Figure 7 Relationship between the trap energy retrieved by the Kissinger method and the nominal energy used in the simulations for a specimen thickness $L=0.25 \text{ mm}$.

Multi peak fit exercise of a thermal desorption experiment

An example of the application of the model to a TDS experiment of an industrially processed AISI 470LI steel (1.4013 according to the reference EN ISO 10088-2) is briefly described. This ferritic stainless steel is fully stabilized with Nb and Ti of composition (in mass %) 0.01% C, 0.4% Si, 24% Cr, Mn<0.40%, Ni<0.30%, Mo<0.20%, 0.01% N, 0.1% Ti and the condition $Ti+Nb \geq 0.2+4 \cdot (C\%+N\%)$.

The sample is a cold rolled strip with a thickness of 3 mm, continuously annealed at 930°C, pickled (both electrochemically and chemically) and skinpassed to achieve a 2B surface finishing. In its final condition, the material exhibits a well recrystallized polygonal ferrite structure with mean grain size of 35 μm .

The TDS of the as-produced steel has been obtained with a heating rate of 250°C/h. The total amount of hydrogen thermally desorbed has been 0.23 ppm by mass. Hydrogen adsorption occurred either during the recrystallization annealing in hydrogen atmosphere or during pickling in acidic solutions (sulfuric and hydrofluoric acid).

The spectrum shown in Figure 8 (redrawn from the original figure in [41] after background subtraction) reveals at least three peaks at approximately 215, 380 and 545°C. The first peak disappears after a thermal treatment at 250°C for 10 hours while the rest of the spectrum remains unchanged. Additionally, specimens annealed in the laboratory to obtain a coarser average grain size, pickled but not skinpassed, do not exhibit the first peak.

This behavior can be reasonably explained by associating the first peak to dislocations introduced by the skinpass treatment, and the peaks at 400 and 545°C to titanium-niobium carbonitrides precipitated along grain boundaries and within the grain interior, as confirmed by metallographic inspection. Conversely, grain boundaries can be associated with reversible traps and do not contribute to the TDS.

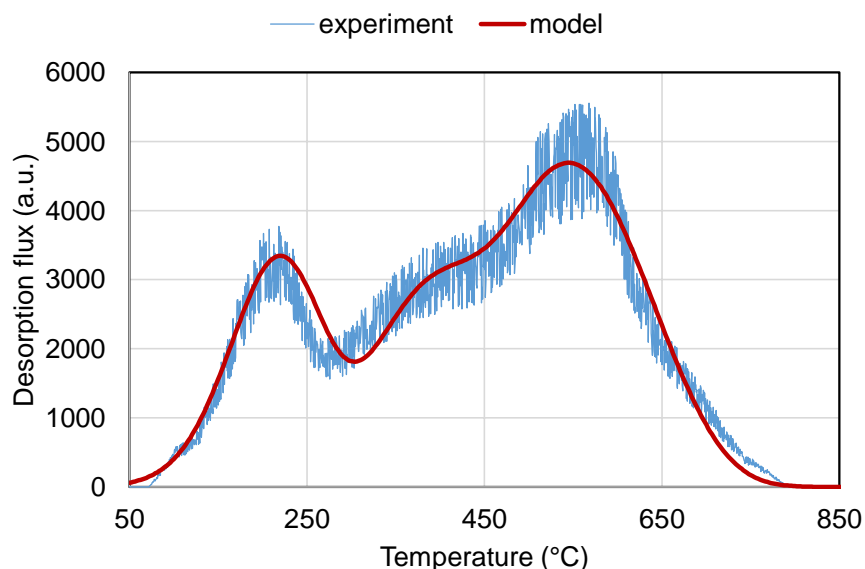


Figure 8 Experimental thermal desorption spectrum of an AISI 470LI steel with superimposed the approximation by the model (smooth solid line).

The experimental desorption curve has been reproduced by the model using a trial-and-error procedure, manually refining the energy and site density of three kinds of traps. A numerical scaling factor has been applied to adapt the calculation results to the measured data. The best result is shown in Figure 8 as a smooth curve superimposed on the measurements.

This exercise allows us to analyze several important aspects of this approach. The first aspect concerns the specimen geometry and size. Typically, cylindrical specimens pre-charged with hydrogen are used in thermal desorption experiments. In contrast, the present model considers a specimen in the form of a thin sheet. Additionally, as previously noted, the specimen thickness influences the temperature and breadth of the desorption peaks, which broaden and shift towards higher temperatures as the thickness L increases (Figure 6). To reproduce the sharp peaks observed in the experiment, it has been necessary to consider a thin specimen with $L=0.1$ mm.

The effect of the specimen size and geometry has been analyzed in the literature [8] [12] and is an aspect that requires careful consideration as many factors can influence the desorption spectrum, such as the initial distribution of the hydrogen within the specimen at the start of thermal desorption.

Another important aspect is the relevance of the absolute values of the energies used in the manual fitting exercise, which in this case are 30 kJ/mol ($N_{30}=4.89 \cdot 10^{21} \text{ m}^{-3}$), 44 kJ/mol ($N_{44}=4.37 \cdot 10^{21} \text{ m}^{-3}$) and 65 kJ/mol ($N_{65}=1.18 \cdot 10^{22} \text{ m}^{-3}$). Specifically, the associated density of trap sites has been set to obtain a residual amount of hydrogen after free desorption matching that determined by the TDS measurement and fulfilling the constraint imposed by the relative height of desorption peaks. The trap energies have been then adjusted to align with the experimental peaks.

As discussed in the previous section, the Kissinger method is a reliable procedure for deducing the trap energy from the temperature of peaks observed at different heating rates. However, a single desorption experiment, even if well reproduced by a model, can only provide an approximate estimation of the binding energies.

This desorption calculation also provides an opportunity to analyze another set of data generated by the model: the evolution of the trap sites occupancy in a multi-trap system. The profiles shown in Figure 9 reveal interesting features indicative of the complex desorption kinetics resulting from interactions among the trap sites. Traps with the lowest energy are depleted first, but the depletion profile as a function of temperature exhibits undulations, of progressively smaller intensity, slowing down their depletion as the lattice hydrogen concentration increases. The smoothest profile is associated with traps possessing the highest energy. This is caused by interaction with desorption from higher energy traps as they begin to release hydrogen. It should be noted that the effect is limited as it affects the occupancy fractions below 0.1 and is graphically magnified by the logarithmic scale in the plot.

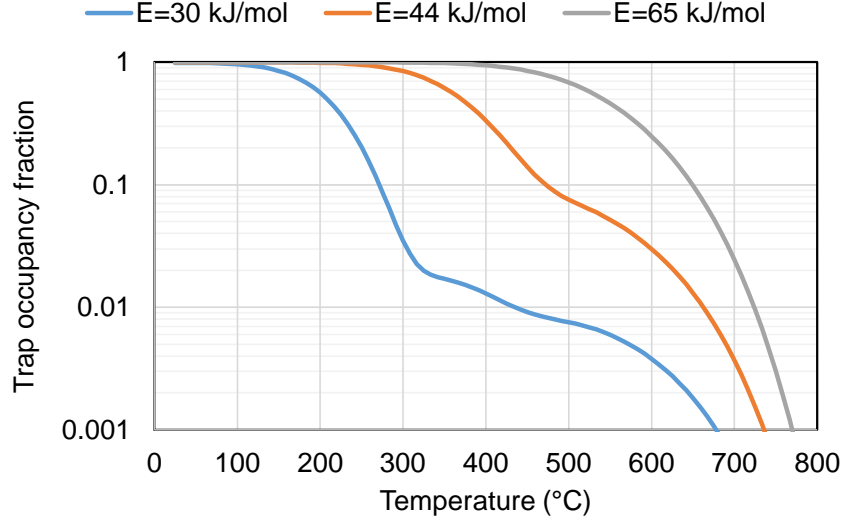


Figure 9 Calculated evolution of the trap occupancy fraction as a function of the temperature during thermal desorption and of the trap binding energy.

Discussion

The simulations presented in the previous sections show that the model behaves consistently and can reproduce all the main theoretical features derived from the approximate analytical solution of the permeation process. Furthermore, when applied to thermal desorption, it has elucidated the effects of trap density, binding energy and specimen thickness on the position of desorption peaks suggesting that the Kissinger method is the only reliable technique for estimating the trap energy from the experiments.

The model provides an opportunity to delve deeper into certain theoretical aspects of the permeation tests by exploiting the knowledge of the main physical quantities characterizing the system, namely trap density and energy.

Based on the data in Table 2 and considering the observations made on equation (17), it has been attempted to empirically derive an expression relating the time lag to the cathodic concentration and trap density. The simulations employed to this purpose have been conducted on ideal systems containing two kinds of traps: a low-energy (20 kJ/mol) and high energy (≥ 40 kJ/mol) with an average site ratio of 94:6. The analytical expression has been designed using dimensional arguments and by analogy with the classical definition of D_{app} , by considering a pre-factor $L^2/6 D_H$ expressing the minimum permeation time in absence of traps. Subsequently, to account for the physical dependence of time lag on the cathodic concentration and on the trap occupancy in stationary flux conditions, a direct proportionality to the fraction of occupied traps and an inverse dependence on the concentration of hydrogen on the cathodic side have been considered, based on the simulation results and elementary physical reasoning. Hence, the simplest relationship compatible with the boundary condition in a trap-free system should be in the form:

$$t_L = \frac{L^2}{6 D_H} \cdot \left(1 + \frac{\sum_j y_{Tj} N_{Tj}}{N_0/2} \right) \quad (21)$$

The sum in the numerator represents the number of the occupied trap sites per unit volume assuming that the occupancy of lattice sites is negligible compared to that of the traps and $N_0 = 8.47 \cdot 10^{22} \cdot c_0 (ppm)$ is the concentration of hydrogen at the cathodic side in m^{-3} . The quantity $N_0/2$ represents the mean concentration within the entire specimen in a stationary flux regime characterized by a linear profile with c_0 at the cathodic side and zero at the anodic side. The trap occupancy fraction can be considered equal to unity for binding energies greater than or equal to 40 kJ/mol, whereas for the low energy traps (20 kJ/mol), it depends on the cathodic concentration. Instead of using the precise occupancy fraction of low-energy traps obtained directly from the simulations, the saturation degree has been approximated with excellent accuracy by the classical relationship describing the equilibrium adsorption/desorption kinetics [3] analogous to equation (1):

$$y_{20} = \frac{(y_0/2) \cdot \exp\left\{+\frac{E}{RT}\right\}}{1 + (y_0/2) \cdot \exp\left\{+\frac{E}{RT}\right\}} \quad (22)$$

where $y_0 = 55.85 \cdot 10^{-6} \cdot c_0 (ppm)$ is the lattice occupancy fraction at the cathodic side and the equilibrium constant contains the energy E considered as a fitting parameter.

In the present case the energy is found to be approximately 34 kJ/mol, which is slightly higher than the expected nominal value of 20 kJ/mol. This discrepancy can be considered of minor relevance given the approximations made, particularly the fundamental asymmetry between adsorption and desorption of this model compared to Oriani's symmetric approach, and the overall objective of this discussion. Furthermore, the agreement between the calculated trap occupancy as a function of the lattice concentration and the theoretical equilibrium expression provides additional confirmation of the model's consistency.

The comparison between the time lag derived from the model simulations of permeation and that obtained from the proposed relationship spans a data range from a few seconds up to approximately 16 hours, yielding a surprisingly high correlation coefficient of 0.994, as illustrated in Figure 10.

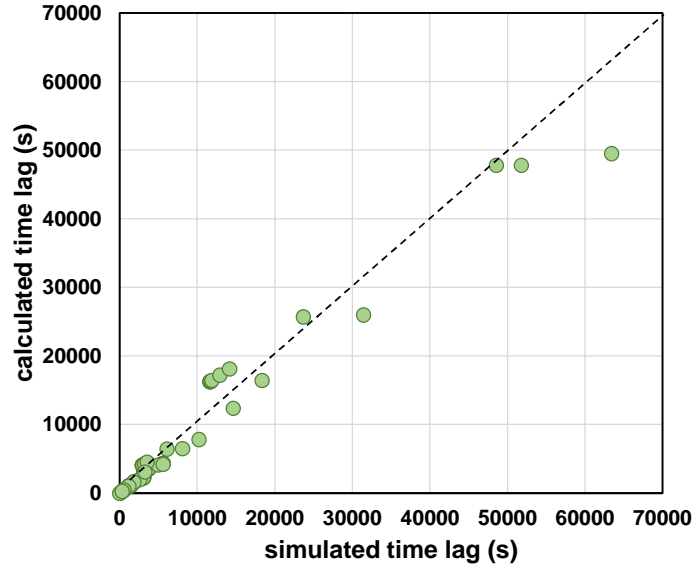


Figure 10 Scatter plot between the proposed empirical estimate of time lag and the value determined from the calculated permeation curve.

It can be observed that by eliminating the time lag in the above relationship by exploiting its usual definition, $t_L = L^2 / 6 D_{app}$, one obtains:

$$\frac{D_{app}}{D_H} = \left(1 + \frac{\sum_j y_{Tj} \cdot N_{Tj}}{N_0/2} \right)^{-1} \quad (23)$$

which qualitatively resembles the result of Oriani's analysis for deducing the binding energy and density of *reversible traps* from permeation experiments:

$$\frac{D_{app}}{D_H} = \left(1 + \frac{N_T}{N_L} \cdot \exp \left\{ + \frac{E_T}{RT} \right\} \right)^{-1} \quad (24)$$

Once again, the differences are in the empirical procedure used to derive equation (21) and primarily in the introduction of the explicit dependence on the cathodic concentration.

To conclude, equation (17) can be rewritten to express the time lag obtaining:

$$t_L = \frac{L^2}{6 D_H} \cdot \frac{c_0^*}{c_0} \quad (25)$$

By analogy with equation (21) it permits, after some rearrangements, to derive an estimate of c_0^* of the form:

$$c_0^*(ppm) = c_0 + 2.36 \cdot 10^{-23} \cdot \sum_j y_{Tj} \cdot N_{Tj} \quad (26)$$

which suggest that both the cathodic concentration and trap occupancy contribute to determining the Oriani's subsurface cathodic concentration.

It might be insightful to add a final comment on topological aspects related to traps, at least from a qualitative perspective.

In all model formulations from the literature, including the present one, there is no explicit mention of the relationship between the topology of trap sites and the trapping-detrapping kinetics. In reality, the dimensionality of possible trap sites spans a wide range of values. Point defects (vacancies) are zero-dimensional sites, dislocations are one-dimensional defects, while grain boundaries, interfaces of precipitates and second phases in general have a two-dimensional character. Moreover, grain boundaries are in contact with the matrix on both sides, whereas second phases are only in contact with the matrix on one side. Additionally, the grain boundary character associated with their relative misorientation could also have an effect.

This could necessitate the introduction of additional factors, of the order of unity, to account for further differences in reaction rates among the different types of traps.

Conclusions

The proposed model, derived from the approach by McNabb and Foster, features an entirely physical formulation without any calibration parameters. It enables the simulation of permeation, free desorption, and thermal desorption within the same theoretical framework. The kinetic equations upon which it is based require only the number density of the different types of traps and their associated binding energies. The meaning of all factors appearing in the equations is clearly explained and justified through statistical and probabilistic arguments. Suggestions regarding the numerical procedure developed to solve the overall kinetics are also provided.

The model correctly reproduces the physics of the system and the results of classical analytical solutions of the permeation kinetics. It is also capable of reproducing thermal desorption spectra with considerable accuracy.

The sensitivity analysis has elucidated the relationships among processing conditions and the typical parameters of the classical analysis of permeation experiments. Specifically, a relationship expressing the dependence of the time lag in permeation on specimen thickness, number density of occupied trap sites and cathodic concentration is proposed. Although empirically derived from the simulated data, this relationship has demonstrated a good capability of predicting the time lag over a range spanning approximately five orders of magnitude.

In summary, the model represents a valuable tool in supporting the interpretation and rationalization of the experiments also from a quantitative viewpoint.

References

- [1] L.S. Darken, R.P. Smith, Behavior of Hydrogen in Steel During and After Immersion in Acid, Corrosion 5 (1949) 1–16. 10.5006/0010-9312-5.1.1
- [2] A. McNabb, P.K. Foster, A new analysis of diffusion of hydrogen in iron and ferritic steels, Trans. Metall. Soc. AIME 227 (1963) 618-627.

- [3] R.A. Oriani, The diffusion and trapping of hydrogen in steel, *Acta Metall.* 18 (1970) 147-157. 10.1016/0001-6160(70)90078-7
- [4] T.-Y. Zhang Y.-P. Zheng, Effects of absorption and desorption on hydrogen permeation. Theoretical modeling and room temperature verification, *Acta Mater.* 46 (1998) 5023-5033. 10.1016/S1359-6454(98)00176-1
- [5] T.-Y. Zhang, I. Wat, Characterization of isolated hydrogen traps by hydrogen permeation experiments, *J. Appl. Phys.* 93 (2003), 6016-6024. 10.1063/1.1565493
- [6] F.D. Fischer, G. Mori, J. Svoboda, Modelling the influence of trapping on hydrogen permeation in metals, *Corrosion Science* 76 (2013) 382–389. 10.1016/j.corsci.2013.07.010
- [7] E.J. Song, D.-W. Suh, H.K.D.H. Bhadeshia, Theory for hydrogen desorption in ferritic steel, *Computational Materials Science* 79 (2013) 36–44. 10.1016/j.commatsci.2013.06.008
- [8] M. Enomoto, D. Hirakami, Influence of Specimen Thickness on Thermal Desorption Spectrum of Hydrogen in High Strength SCM435 Steel, *ISIJ International* 55 (2015), 2492-2498. 10.2355/isijinternational.ISIJINT-2015-345
- [9] E.K. Kostikova and Yu.V. Zaika, Modelling of hydrogen thermal desorption spectrum in nonlinear dynamical boundary-value problem, *J. Phys.* (2016): Conf. Ser. 769 012024. 10.1088/1742-6596/769/1/012024
- [10] M.A. Stopher, P. Lang, E. Kozeschnik, P.E.J. Rivera-Diaz-del-Castillo, Modelling hydrogen migration and trapping in steels, *Materials & Design* 106 (2016) 205-215. 10.1016/j.matdes.2016.05.051
- [11] L. Cheng, L. Li, X. Zhang, J. Liu, K. Wu, Numerical simulation of hydrogen permeation in steels, *Electrochimica Acta* 270 (2018) 77-86. 10.1016/j.electacta.2018.03.061
- [12] Y. Wang, S. Hu, G. Cheng Effect of Specimen Geometry on the Thermal Desorption Spectroscopy Evaluated by Two-Dimensional Diffusion-Trapping Coupled Model, *Materials* 2021, 14(6), 1374. 10.3390/ma14061374
- [13] K.-i. Ebihara, Y. Sugiyama, R. Matsumoto, K. Takai, T. Suzudo, Numerical Interpretation of Hydrogen Thermal Desorption Spectra for Iron with Hydrogen-Enhanced Strain-Induced Vacancies, *Metall. Mater. Trans. A* 52 (2021) 257–269. 10.1007/s11661-020-06075-7
- [14] F. Montupet-Leblond, L. Corso, M. Payet, R. Delaporte-Mathurin, E. Bernard, Y. Charles, J. Mougnot, S. Vartanian, E.A. Hodille, C. Grisolia, Permeation and trapping of hydrogen in Eurofer97. *Nuclear Materials and Energy* 29 (2021) 101062. 10.1016/j.nme.2021.101062.
- [15] K.-i. Ebihara, D. Sekine, Y. Sakiyama, J. Takahashi, K. Takai, T. Omura, Numerical interpretation of thermal desorption spectra of hydrogen from high-carbon ferrite-austenite dual-phase steel, *Int. J. of Hydrogen Energy* 48 (2023) 30949-30962. 10.1016/j.ijhydene.2023.04.205
- [16] S. Zheng, Y. Qin, W. Li, F. Huang, Y. Qiang, S. Yang, L. Wen, Y. Jin, Effect of hydrogen traps on hydrogen permeation in X80 pipeline steel - a joint experimental and modelling study, *Int. J. of Hydrogen Energy* 48 (2023) 4773-4788. 10.1016/j.ijhydene.2022.10.038
- [17] M.A.V. Devanathan, L. Stachurski, The adsorption and diffusion of electrolytic hydrogen in palladium. *Proc. R. Soc. (London)* A270 (1962) 90–102. 10.1098/rspa.1962.0205

- [18] M.A.V. Devanathan, L. Stachurski, The mechanism of hydrogen evolution on iron in acid solutions by determination of permeation rates. *J. Electrochem. Soc.* 111 (1964) 619–623. 10.1149/1.2426195
- [19] H. Eyring, The Activated Complex in Chemical Reactions. *J. Chem. Phys.* 3 (1935) 107–115. 10.1063/1.1749604
- [20] C. Capdevila, F.G. Caballero, C. García De Andrés, “Isothermal allotriomorphic ferrite formation kinetics in a medium carbon vanadium-titanium microalloyed steel”, *Scripta Materialia*, 44 (2001) 593–600. 10.1016/S1359-6462(00)00647-3
- [21] G.M. Pressouyre, I.M. Bernstein, A quantitative analysis of hydrogen trapping, *Metall. Trans. A* 9 (1978) 1571–1580. doi.org/10.1007/BF02661939
- [22] G. Pressouyre, A Classification of Hydrogen Traps in Steel, *Metall. Trans. -Phys. Metall. Mater. Sci.*, 10 (1979) 1571–1573. 10.1007/BF02812023.
- [23] J.P. Hirth, Effects of hydrogen on the properties of iron and steel, *Metallurgical and Materials Transactions A* 11 (1980) 861–890. 10.1007/BF02654700
- [24] W.Y. Choo and J.Y. Lee, Thermal analysis of trapped hydrogen in pure iron, *Metall. Trans. A*, 13A (1982), 135–140. 10.1007/BF02642424
- [25] H.G. Lee, J.Y. Lee, Hydrogen trapping by TiC particles in iron, *Acta Metall.*, 32 (1984), 131–136. 10.1016/0001-6160(84)90210-4
- [26] H. Hagi, Y. Hayashi, Effect of interstitial impurities on hydrogen trapping by dislocations in iron, *J. Japan. Inst. Met.* 51 (1987), 24–30 (in Japanese).
- [27] N. Parvathavarthini, S. Saroja, R.K. Dayal, H.S. Khatak, Studies on hydrogen permeability of 2.25% Cr-1% Mo ferritic steel: Correlation with microstructure, *Journal of Nuclear Materials*, 288 (2001) 187–196. 10.1016/S0022-3115(00)00706-6
- [28] H. Asahi, D. Hirakami, S. Yamasaki, Hydrogen Trapping Behavior in Vanadium-added Steel, *ISIJ International*, 43 (2003) 527–533. 10.2355/isijinternational.43.527
- [29] F.G. Wei, T. Hara, K. Tsuzaki, Precise Determination of the Activation Energy for Desorption of Hydrogen in Two Ti-Added Steels by a Single Thermal-Desorption Spectrum, *Metall. Mater. Trans. B* 35B (2004) 587–597. 10.1007/s11663-004-0057-x
- [30] S. Frappart, X. Feaugas, J. Creus, F. Thébault, L. Delattre, H. Marchebois, Study of the hydrogen diffusion and segregation into Fe–C–Mo martensitic HSLA steel using electrochemical permeation test. *J. Phys. Chem. Solids* 71 (2010) 1467–1479. 10.1016/j.jpcs.2010.07.017
- [31] D. Gaude-Fugarolas, Effect of microstructure and trap typology on hydrogen redistribution in steel, *Proceedings of METAL 2013*, Brno, Czech Republic (May 2013) 15–17.
- [32] J. Sanchez, A. Ridruejo, P.L. de Andres, Diffusion and trapping of hydrogen in carbon steel at different temperatures, *Theoretical and Applied Fracture Mechanics* 110 (2020) 102803. 10.1016/j.tafmec.2020.102803
- [33] Y.-S. Chen, C. Huang, P.-Y. Liu, H.-W. Yen, R. Niu, P. Burr, K.L. Moore, E. Martínez-Pañeda, A. Atrens, J.M. Cairney, Hydrogen trapping and embrittlement in metals – A review, *International Journal of Hydrogen Energy*, in press. 10.1016/j.ijhydene.2024.04.076
- [34] K. Kiuchi, R.B. McLellan, The solubility and diffusivity of hydrogen in well annealed and deformed iron, *Acta Metall.* 31 (1983) 961–984. 10.1016/0001-6160(83)90192-X

- [35] A. Turnbull, Hydrogen diffusion and trapping in metals, in “Gaseous HE of materials in energy technologies”, Chapter 4, Woodhead Publishing Limited, 2012.
- [36] F. Huang, J. Liu, Z.J. Deng, J.H. Cheng, Z.H. Lu, X.G. Li, Effect of microstructure and inclusions on hydrogen induced cracking susceptibility and hydrogen trapping efficiency of X120 pipeline steel, *Materials Science and Engineering A*, 527(2010) 6997-7001. 10.1016/j.msea.2010.07.022
- [37] M. Skjellerudsveen, O.M. Akselsen, V. Olden, R. Johnsen, A. Smirnova, Effect of Microstructure and Temperature on Hydrogen Diffusion and Trapping in X70 grade Pipeline Steel and its Weldments, 2010. https://ntnuopen.ntnu.no/ntnu-xmlui/bitstream/handle/11250/241468/506329_FULLTEXT01.pdf?sequence=1
- [38] Q. Cui, J. Wu, D. Xie, X. Wu, Y. Huang, X. Li, Effect of Nanosized NbC Precipitates on Hydrogen Diffusion in X80 Pipeline Steel, *Materials* 10 (2017) 721. 10.3390/ma10070721
- [39] A. Thomas, J.A. Szpunar, Hydrogen diffusion and trapping in X70 pipeline steel, *International Journal of Hydrogen Energy*, 45, (2020) 2390-2404. 10.1016/j.ijhydene.2019.11.096
- [40] H.E. Kissinger, Reaction Kinetics in Differential Thermal Analysis. *Analytical Chemistry*, 29 (1957) 1702-1706. 10.1021/ac60131a045
- [41] P. Neri, P.E. Di Nunzio, A. De Vito, RC-CSM internal report no. P0037386-1-H1 Rev.0 (2024).